Exponentially Stretching Sheet in a Powell–Eyring Fluid: Numerical and Series Solutions

Ammar Mushtaq[a], Meraj Mustafa[a], Tasawar Hayat[b,c], Mahmood Rahi[d], and Ahmed Alsaedi[c]

[a] Research Centre for Modeling and Simulation (RCMS), National University of Sciences and Technology (NUST), Islamabad 44000, Pakistan
[b] Department of Mathematics, Quaid-i-Azam University 45320, Islamabad 44000, Pakistan
[c] Nonlinear Analysis and Applied Mathematics (NAAM) Research Group, King Abdulaziz University, Jeddah 21589, Saudi Arabia
[d] National University of Sciences and Technology (NUST), Islamabad 44000, Pakistan

Reprint requests to M. M.; Tel: +92 51 90855733, E-mail: meraj_mm@hotmail.com

Z. Naturforsch. **68a,** 791 – 798 (2013) / DOI: 10.5560/ZNA.2013-0063
Received May 15, 2013 / revised August 14, 2013 / published online October 16, 2013

This work theoretically examines the flow and heat transfer characteristics due to an exponentially stretching sheet in a Powell–Eyring fluid. Governing partial differential equations are non-dimensionalized and transformed into non-similar forms. Explicit analytic expressions of velocity and temperature functions are developed by homotopy analysis method (HAM). The Numerical solutions are obtained by using shooting method with fourth-order Runge–Kutta integration technique. The fields are influence appreciably with the variation of embedding parameters. We noticed that the velocity ratio has a dual behaviour on the momentum boundary layer. On the other hand the thermal boundary layer thins when the velocity ratio is increased. The results indicate a significant increase in the velocity and a decrease in thermal boundary layer thickness with an intensification in the viscoelastic effects.

Key words: Exponentially Stretching Sheet; Powell–Eyring Fluid; Shooting Method; Stagnation-Point Flow; Heat Transfer; Series solution.

1. Introduction

Recent advancements in technological and engineering applications have brought a wide range of non-Newtonian fluids that are characterized by diverse significant deviations from the viscous fluids. Examples of such fluids include coal water or coal-oil slurries, food products, inks, glues, soaps, shampoos, certain paints, polymer solutions etc. In these fluids, the relationship between the shear stress and flow field is very complicated. The viscoelastic properties add more complexities in the resulting nonlinear equations. Several researchers are presently engaged in the flow analysis of non-Newtonain fluids. The Powell–Eyring fluid model is mathematically complex but it has certain advantages over other non-Newtonian fluid models. Firstly, it is deduced from kinetic theory of liquid rather than the empirical relation and, secondly, it correctly reduces to Newtonian behaviour for low and high shear rates. It has been seen that the Powell–Eyring fluid model is better to formulate the flows of modern industrial materials such as powdered graphite and ethylene glycol. The analysis of a Powell–Eyring fluid flow has been scarcely discussed in the literature despite of the complexities associated with the explicit expressions of stress components and velocity. Influence of couple stresses on the flow of a Powell–Eyring fluid between parallel plates was investigated by Eldabe et al. [1]. Zueco and Beg [2] numerically investigated the pulsatile flow of a Powell–Eyring fluid by an explicit finite difference scheme. Homotopy perturbation analysis of slider bearing lubricated with a Powell–Eyring fluid is presented by Islam et al. [3]. Patel and Timol [4] numerically examined the flow of a Powell–Eyring model past a wedge by using the method of satisfaction of asymptotic boundary conditions. Analytic solutions for flow of a Powell–Eyring fluid over a continuously moving surface with convective boundary conditions are computed by Hayat et al. [5].

The study of flow and heat transfer due to extensible surfaces has obvious importance in industry and

engineering. In fact various technical processes related to polymers involve the production of sheeting material which includes both metal and polymer sheets. The quality of the final product depends on the heat transfer rate at the stretching surface. The pioneering work on the two-dimensional flow over a flat moving surface was reported by Sakiadis [6]. Crane [7] extended this idea for a stretching sheet and provided an exact solution of the arising differential system. The researchers have looked at Crane's problem under various aspects (see Rajagopal et al. [8], Mahapatra and Gupta [9], Cortell [10], Bachok et al. [11], Abbasbandy and Ghehsareh [12], Fang et al. [13], Hayat et al. [14], Mustafa et al. [15, 16], Bhattacharyya and Layek [17] etc.). However the flow analysis over an exponentially stretching sheet is sparsely studied. Magyari and Keller [18] discussed the heat and mass transfer effects on the flow of a viscous fluid over an exponentially stretching sheet. The characteristics of suction and heating scheme on an exponentially stretched flow have been analyzed by Elbashbeshy [19]. The boundary layer flow of a viscoelastic fluid over an exponentially stretching sheet is addressed by Khan and Sanjayanand [20]. The effect of thermal radiation on the flow due to an exponentially stretching surface in a viscous fluid has been examined by Sajid and Hayat [21]. Boundary layer flow and heat transfer of a second-grade fluid over an exponentially stretching sheet are investigated by Nadeem et al. [22].

To the best of our knowledge, there is not a single article in the literature that addresses the flow of a Powell–Eyring fluid due to an exponentially stretching surface. Therefore we present a mathematical model for stagnation-point flow and heat transfer due to an exponentially stretching sheet in a Powell–Eyring fluid. Such analysis in absence of stagnation point and heat transfer has not been yet reported. The equations are first modelled and then solved numerically using the shooting method with Runge–Kutta algorithm. It is quite obvious that numerical solutions can only be obtained for discrete set of points. Therefore it is occasionally time consuming to get a complete curve of results. On the other hand the analytic solutions, available in the complete domain of interest and having a reasonable amount of accuracy, are always handy for scientists and engineers. The present problem is therefore also solved analytically in the whole spatial domain $(0 \leq \eta < \infty)$ by using an efficient analytical tool namely the homotopy analysis method (HAM). The analytic solutions are found in excellent agreement with the numerical solutions for all the values of embedded parameters. The accuracy of HAM has already been verified for various nonlinear problems in science and engineering [23 – 35]. Latest advances in homotopy analysis method can be sought from Liao [36]. Interpretation to the physical parameters is assigned through graphical and numerical results. The dimensionless expressions of skin friction coefficient and local Nusselt number are evaluated and discussed.

2. Formulation of the Problem

We consider the incompressible flow of a Powell–Eyring fluid over an exponentially stretching sheet. The x- and y-axis are taken along and perpendicular to the sheet and the flow is confined to $y \geq 0$. Let $U_{\mathrm{w}}(x) = a\exp(x/l)$ denote the velocity of the sheet while the velocity of external flow is $U_\infty(x) = b\exp(x/l)$. In view of polymer extrusion, the material properties and in particular the elasticity of the extruded sheet is being pulled out by a constant force. Let $T_{\mathrm{w}}(x) = T_\infty + c\exp(x/2l)$ denote the temperature of the surface where T_∞ is the ambient temperature. In the absence of heat generation and viscous dissipation, the steady boundary layer equations for flow and heat transfer in a Powell–Eyring fluid are (see Patel and Timol [4] and Hayat et al. [5])

$$\frac{\partial u}{\partial x} + \frac{\partial v}{\partial y} = 0\,, \tag{1}$$

$$u\frac{\partial u}{\partial x} + v\frac{\partial u}{\partial y} = U_\infty \frac{\mathrm{d}U_\infty}{\mathrm{d}x} + \left(\nu + \frac{1}{\rho\beta C}\right)\frac{\partial^2 u}{\partial y^2} - \frac{1}{2\rho\beta C^3}\left(\frac{\partial u}{\partial y}\right)^2 \frac{\partial^2 u}{\partial y^2}\,, \tag{2}$$

$$u\frac{\partial T}{\partial x} + v\frac{\partial T}{\partial y} = \frac{k}{\rho C_{\mathrm{p}}}\frac{\partial^2 T}{\partial y^2}\,, \tag{3}$$

where ν is the kinematic viscosity, ρ is the fluid density, u and v are the velocity components in x- and y-directions, respectively, β and C are the material fluid parameters, C_{p} is the specific heat at constant pressure, T is the fluid's temperature and k is the thermal conductivity.

The relevant boundary conditions are

$$\begin{aligned} &u = U_{\mathrm{w}}(x) = a\exp(x/l)\,,\ \ v = 0\,,\\ &T = T_{\mathrm{w}}(x) = T_\infty + c\exp(x/2l) \text{ at } y = 0\,,\\ &u \to U_\infty(x) = b\exp(x/l)\,,\ \ T \to T_\infty \text{ as } y \to \infty\,. \end{aligned} \tag{4}$$

Inserting the following similarity transformations

$$\eta = \sqrt{\frac{a}{2\nu L}}\,\mathrm{e}^{x/2L} y,\ \ u = a\,\mathrm{e}^{x/L} f'(\eta),$$
$$v = -\sqrt{\frac{\nu a}{2L}}\,\mathrm{e}^{x/2L}\left[f(\eta)+\eta f'(\eta)\right], \tag{5}$$
$$\theta(\eta) = \frac{T-T_\infty}{T_\mathrm{w}-T_\infty}$$

into (2)–(4), we have

$$(1+K)\,f''' + f f'' - 2f'^2 - K\Gamma f''^2 f''' + 2\lambda^2 = 0, \tag{6}$$
$$\theta'' + \mathrm{Pr}\left(f\theta' - \theta f'\right) = 0, \tag{7}$$
$$f(0)=0,\ \ f'(0)=1,\ \ \theta(0)=1,$$
$$f'(\infty)\to\lambda,\ \ \theta(\infty)\to 0. \tag{8}$$

In the above equations, λ is the velocity ratio, K and Γ are the dimensionless fluid parameters, and Pr is the Prandtl number. These are defined as

$$\lambda = \frac{b}{a},\ \ K = \frac{1}{\mu\beta C},\ \ \Gamma = \frac{U_\mathrm{w}^3}{4\nu L C^2},\ \ \mathrm{Pr} = \frac{\mu C_\mathrm{p}}{k}. \tag{9}$$

In is worth mentioning here that the governing differential system does not exhibit a self-similar solution since Γ is a function of x. Therefore we look for local similarity solution of (6)–(8) which permits us to investigate the behaviour of parameters at a fixed location above the sheet. Further when $K=0$, equations of motion for the viscous (Newtonian) fluid case are recovered. The physical quantities of interest here are the skin friction coefficient C_f and local Nusselt number Nu defined as

$$C_\mathrm{f} = \frac{\tau_\mathrm{w}}{\rho U_\mathrm{w}^2},\ \ \mathrm{Nu} = \frac{x q_\mathrm{w}}{(T_\mathrm{w}-T_\infty)}, \tag{10}$$

where τ_w is the wall shear stress and q_w is the surface heat flux given by

$$\tau_\mathrm{w} = \left(\mu+\frac{1}{\beta C}\right)\left.\frac{\partial u}{\partial y}\right|_{y=0} - \left.\frac{1}{6\beta C^3}\left(\frac{\partial u}{\partial y}\right)^3\right|_{y=0},$$
$$q_\mathrm{w} = -k\left.\left(\frac{\partial T}{\partial y}\right)\right|_{y=0}, \tag{11}$$
$$\sqrt{2\mathrm{Re}}\,C_\mathrm{f} = (1+K)\,f''(0) - \frac{K\Gamma}{3}\left(f''(0)\right)^3,$$
$$\sqrt{\frac{2L}{x}}\,\mathrm{Nu}/\mathrm{Re}_x^{1/2} = -\theta'(0), \tag{12}$$

where $\mathrm{Re} = U_\mathrm{w}L/\nu$ and $\mathrm{Re}_x = U_\mathrm{w}x/\nu$ are the local Reynolds numbers.

3. Numerical Method

Equations (6) and (7) subject to the boundary conditions (8) have been solved numerically using the shooting method using fourth-order Runge–Kutta integration technique. However it is required to transform the original differential equations into a system of first-order ordinary differential equations as

$$\frac{\mathrm{d}f}{\mathrm{d}\eta} = F,$$
$$\frac{\mathrm{d}F}{\mathrm{d}\eta} = G, \tag{13}$$
$$\frac{\mathrm{d}G}{\mathrm{d}\eta} = \frac{2F^2 - fG - 2\lambda^2}{1+K-K\Gamma G^2},$$

$$\frac{\mathrm{d}\theta}{\mathrm{d}\eta} = P,$$
$$\frac{\mathrm{d}P}{\mathrm{d}\eta} = -\mathrm{Pr}\,(fP-\theta F) \tag{14}$$

with the boundary conditions

$$f(0)=0,\ \ F(0)=1,\ \ F(\infty)=\lambda,$$
$$\theta(0)=1,\ \ \theta(\infty)=0. \tag{15}$$

In order to integrate (13) and (14) as an initial value problem, we require a value for $G(0)$, i.e. $f''(0)$, and $P(0)$, i.e. $\theta'(0)$, but no such values are given in the boundary. The suitable values for $f''(0)$ and $\theta'(0)$ are chosen and then integration is carried out. We compare the calculated values for f' and θ at $\eta = 10$ (say) with the given boundary condition $f'(10) = a/c$ and $\theta(10) = 0$ and adjust the estimated values, $f''(0)$ and $\theta'(0)$, to get a better approximation for the solution. Different values of η (such as $\eta = 10, 11, 12, 13$ etc.) are taken in our numerical computations so that numerical values are independent of η chosen.

4. Homotopy Analytic Solutions

The rule of solution expression and the involved boundary conditions direct us to select the following initial guesses and auxiliary linear operators:

$$f_0(\eta) = \lambda\eta + (1-\lambda)\,(1-\exp(-\eta)),$$
$$\theta_0(\eta) = \exp(-\eta), \tag{16}$$

$$\mathcal{L}_f \equiv \frac{\mathrm{d}^3}{\mathrm{d}\eta^3} - \frac{\mathrm{d}}{\mathrm{d}\eta},\ \ \mathcal{L}_\theta \equiv \frac{\mathrm{d}^2}{\mathrm{d}\eta^2} - 1. \tag{17}$$

If $p \in [0,1]$ is an embedding parameter and $\hbar$ denotes the non-zero auxiliary parameter, then the generalized homotopic equations corresponding to (6)–(8) are

$$(1-p)\mathcal{L}_f[F(\eta,p)-f_0(\eta)] = p\hbar\mathcal{N}_f[F(\eta,p)]\,, \tag{18}$$

$$(1-p)\mathcal{L}_\theta[\Theta(\eta,p)-\theta_0(\eta)] = p\hbar\mathcal{N}_\theta[F(\eta,p),\Theta(\eta,p)]\,, \tag{19}$$

$$F(\eta;p)|_{\eta=0} = 0\,,\quad \left.\frac{\partial F(\eta;p)}{\partial\eta}\right|_{\eta=0} = 1\,,\quad \left.\frac{\partial F(\eta;p)}{\partial\eta}\right|_{\eta=\infty} = \lambda\,, \tag{20}$$

$$\Theta(\eta;p)|_{\eta=0} = 1\,,\quad \Theta(\eta;p)|_{\eta\to\infty} = 0\,, \tag{21}$$

in which the nonlinear operators $\mathcal{N}_f$ and $\mathcal{N}_\theta$ are

$$\mathcal{N}_f[F(\eta;p)] = (1+K)\frac{\partial^3 F(\eta;p)}{\partial\eta^3} + F(\eta,p)\frac{\partial^2 F(\eta;p)}{\partial\eta^2} - 2\left(\frac{\partial F(\eta;p)}{\partial\eta}\right)^2 - K\Gamma\left(\frac{\partial F(\eta;p)}{\partial\eta}\right)^2\frac{\partial^3 F(\eta;p)}{\partial\eta^3} + 2\lambda^2\,, \tag{22}$$

$$\mathcal{N}_\theta[F(\eta;p),\Theta(\eta;p)] = \frac{1}{\mathrm{Pr}}\frac{\partial^2\Theta(\eta,p)}{\partial\eta^2} + F(\eta;p)\frac{\partial\Theta(\eta;p)}{\partial\eta} - \Theta(\eta;p)\frac{\partial F(\eta;p)}{\partial\eta}\,. \tag{23}$$

Expanding $F(\eta;p)$ and $\Theta(\eta;p)$ using the Taylors series about $p=0$, we have

$$F(\eta;p) = \sum_{m=0}^{\infty} f_m(\eta)p^m\,,\quad f_m(\eta) = \left.\frac{1}{m!}\frac{\partial^m F(\eta;p)}{\partial p^m}\right|_{p=0}\,, \tag{24}$$

$$\Theta(\eta;p) = \sum_{m=0}^{\infty} \theta_m(\eta)p^m\,,\quad \theta_m(\eta) = \left.\frac{1}{m!}\frac{\partial^m \Theta(\eta;p)}{\partial p^m}\right|_{p=0}\,, \tag{25}$$

and the final solutions are retrieved at $p=1$. The functions f_m and θ_m can be obtained through the deformation of (18)–(23). Explicitly mth-order deformation equations corresponding to (18)–(23) are

$$\mathcal{L}_f[f_m(\eta)-\chi_m f_{m-1}(\eta)] = \hbar\mathcal{R}_m^f(\eta)\,, \tag{26}$$

$$\mathcal{L}_\theta[\theta_m(\eta)-\chi_m\theta_{m-1}(\eta)] = \hbar\mathcal{R}_m^\theta(\eta)\,, \tag{27}$$

$$f_m(0)=0\,,\ f_m'(0)=0\,,\ f_m'(\infty)=0\,,\quad \theta_m(0)=0\,,\ \theta_m(\infty)=0\,, \tag{28}$$

$$\mathcal{R}_m^f(\eta) = (1+K)f_{m-1}''' + 2\lambda^2(1-\chi_m) + \sum_{k=0}^{m-1} f_{m-1-k}f_k'' - 2\sum_{k=0}^{m-1} f_{m-1-k}'f_k' - K\Gamma\sum_{k=0}^{m-1} f_{m-1}''\sum_{k=0}^{m-1} f_{k-l}'''f_l''\,, \tag{29}$$

$$\mathcal{R}_m^\theta(\eta) = \frac{1}{\mathrm{Pr}}\theta_{m-1}'' + \sum_{k=0}^{m-1}\left[f_{m-1-k}\theta_k' - \theta_{m-1-k}f_k'\right]\,; \tag{30}$$

$$\chi_m = \begin{cases} 0, & m \le 1,\\ 1, & m > 1. \end{cases} \tag{31}$$

Now (26)–(31) can be easily solved by using symbolic computational softwares such as Mathematica or Maple for $m = 1,2,3,\ldots$ Here it is pertinent to mention that the boundary condition at infinity can be exactly satisfied by means of HAM, but not by the shooting method.

4.1. Error Analysis and Convergence of the Homotopy Solutions

The solutions given by (26)–(31) contain the auxiliary parameter $\hbar$ which can easily adjust and control the convergence of the series solutions. To obtain the suitable value of this parameter, we have plotted the $\hbar$-curves for f and θ at 15th-order of approximations (see Fig.1). Here admissible values of $\hbar$ lie in the flat portion of these curves. For $\lambda = 0.5$, the interval of convergence for f and θ is $[-0.7,-0.2]$. Further the admissible range of $\hbar$ shrinks as the values of the velocity ratio λ are increased. To see the accuracy of solutions, we define the averaged residual errors for functions f and θ (see Liao [24] for details)

$$E_{m,1}(\hbar) = \frac{1}{N}\sum_{i=0}^{K}\left[\mathcal{N}_f\left(\sum_{j=0}^{m} f_j(i\Delta x)\right)\right]^2\,, \tag{32}$$

$$E_{m,2}(\hbar) = \frac{1}{N}\sum_{i=0}^{K}\left[\mathcal{N}_\theta\left(\sum_{j=0}^{m} \theta_j(i\Delta x)\right)\right]^2\,, \tag{33}$$

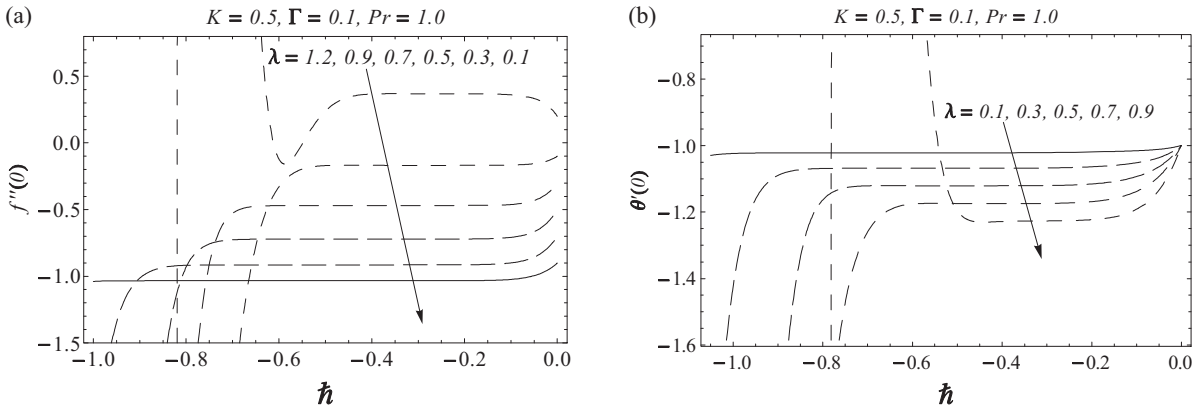

Fig. 1. $\hbar$-curves of (a) $f''(0)$ and (b) $\theta'(0)$ at 15th-order of approximations.

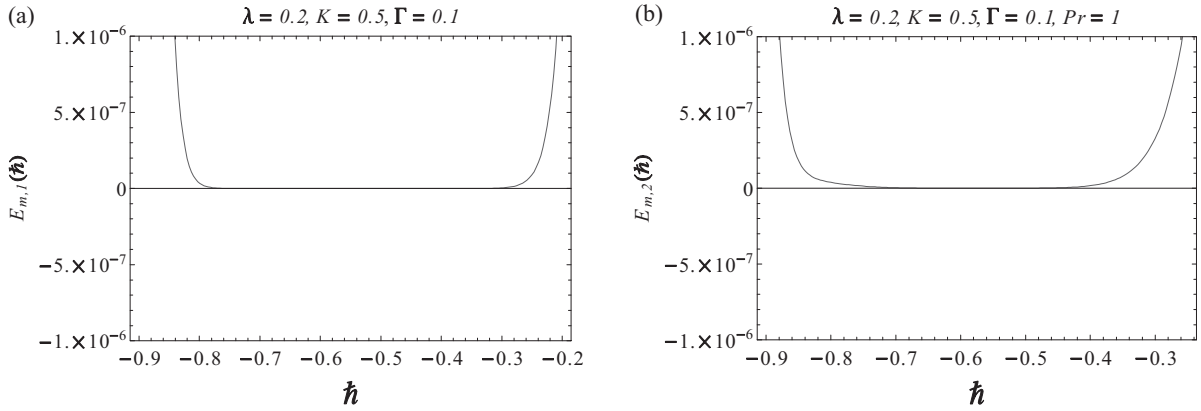

Fig. 2. Averaged residuals for the functions f and θ at 15th-order of approximations.

where $\Delta x = 10/N$ and $N = 20$. The averaged residual errors $E_{m,1}$ and $E_{m,2}$ have been plotted versus $\hbar$ for some fixed values of parameters in Figure 2a and b at 15th-order of approximations. From these curves, we can obtain the best possible values of $\hbar$ by using the command *Minimize* of the software Mathematica.

5. Results and Discussion

In this section, the behaviours of embedding physical parameters on the velocity, temperature, skin friction coefficient, and local Nusselt number are addressed. Graphical results shown in Figures 3 – 8 are obtained by HAM. Figure 3 shows the effect of velocity ratio parameter λ on the velocity and the boundary layer thickness. The velocity being a strong function of λ increases with an increase in λ. When $\lambda > 1$, the thickness of the boundary layer decreases with an increase in λ. Here the straining motion near the stagnation region increases so the acceleration of the external stream increases which causes a reduction in the boundary layer thickness and as a consequence the horizontal velocity increases. On the other hand, when $\lambda < 1$, the flow has an inverted boundary layer structure. Here the sheet velocity $U_w(x)$ exceeds the velocity of external stream $U_\infty(x)$. It is found that a boundary layer is not formed for $\lambda = 1$. The influence of fluid parameter K on the velocity is observed in Figure 4. An increase in K may be either regarded as a decrease in the viscosity or a decrease in rheological effects of the Powell–Eyring fluid. Here we notice that velocity and boundary layer thickness are increasing functions of K when $\lambda < 1$. This observation leads to the conclusion that the increase in the elastic effects of

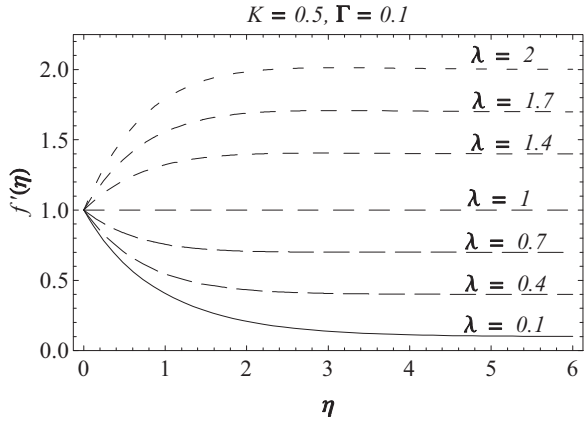

Fig. 3. Influence of λ on f'.

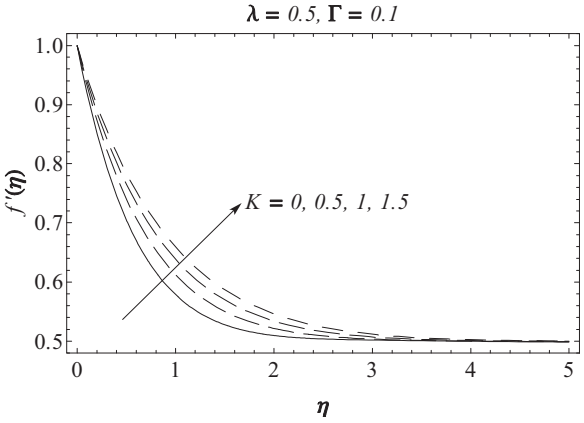

Fig. 4. Influence of K on f'.

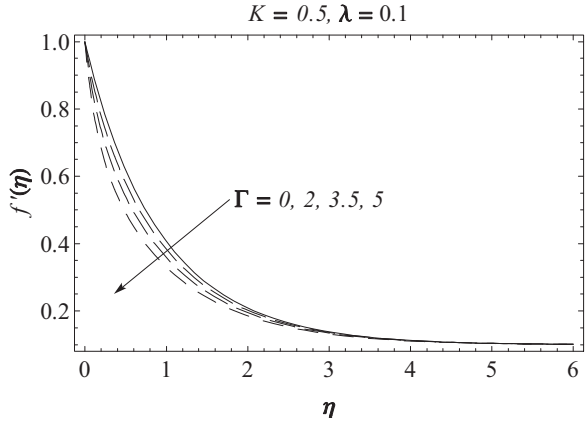

Fig. 5. Influence of Γ on f'.

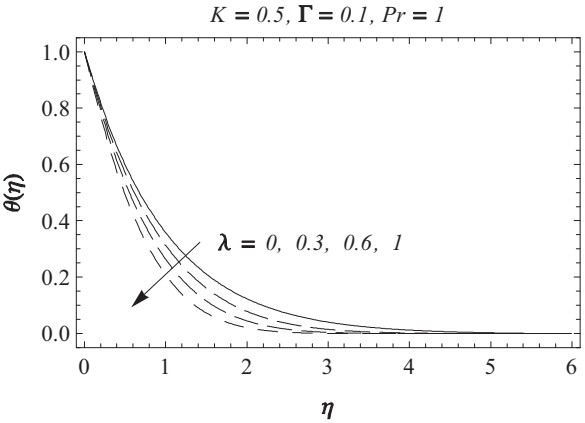

Fig. 6. Influence of λ on θ.

the Powell–Eyring fluid leads to a thinner momentum boundary layer. However an opposite trend is noticed when $\lambda > 1$. Figure 5 is plotted to perceive the effects of dimensionless fluid parameter Γ on the velocity. It is seen that when $\lambda < 1$, an increase in Γ shifts the profiles towards the boundary indicating a diminution in the boundary layer thickness. This notion is quite understandable since an increase in Γ accompanies with a decrease in kinematic viscosity.

Figures 6–8 plot the temperature profiles versus η for various values of parameters. Figure 6 shows that the temperature θ is a decreasing function of λ. This outcome may be inferred to the conclusion that a larger velocity of the sheet corresponds to the thicker thermal boundary layer. There is a slight decrease in the temperature θ when K is increased, and the temperature θ is negligibly affected by varying Γ (see Fig.7). Here unlike the velocity distributions, the parameters have a similar behaviour on the thermal boundary layer and rate of heat transfer at the sheet for all the values of λ. Due to the absence of viscous dissipation effects, the fluid parameters K and Γ are not directly involved in the energy equation, and therefore these parameters have a smaller impact on the thermal boundary layer. Figure 8 indicates that the temperature profiles move towards the boundary when Pr is increased causing a reduction in the thermal boundary layer thickness. Physically this is attributed to the fact that a larger Prandtl number has a relatively lower thermal diffusivity. Thus an increase in Pr reduces the conduction and thereby increases the variation in the thermal characteristics. In other words the profiles become increas-

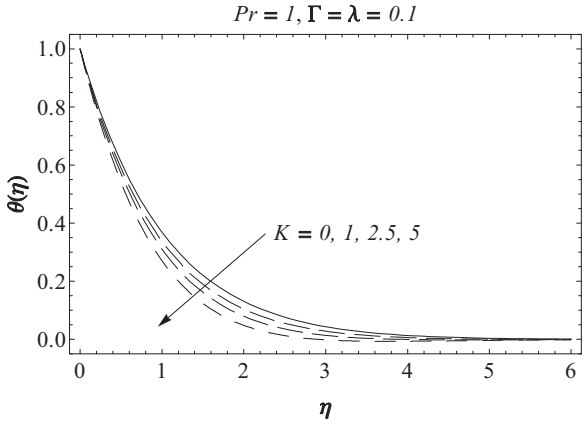

Fig. 7. Influence of K on θ.

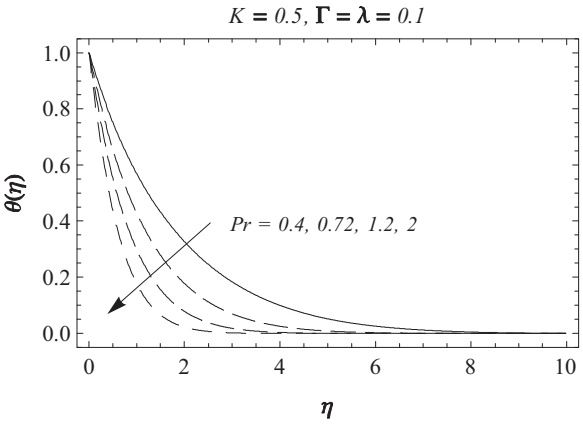

Fig. 8. Influence of Pr on θ.

K	Γ	λ	$\mathrm{Re}_x^{1/2}C_\mathrm{f}$		$\sqrt{\frac{2L}{x}}\mathrm{Nu}/\mathrm{Re}_x^{1/2}$	
			HAM	Numerical	HAM	Numerical
0.0	0.1	0.1	−1.253580	−1.253590	0.977953	0.977955
0.5			−1.530419	−1.530420	1.022158	1.022158
1.0			−1.766459	−1.766456	1.050549	1.050549
1.5			−1.975250	−1.975260	1.070644	1.070644
0.5	0.0		−1.535315	−1.535315	1.023016	1.023016
	0.5		−1.509342	−1.509342	1.018406	1.018406
	1.0		−1.478121	−1.478140	1.012648	1.012648
	1.5		−1.414220	−1.413130	1.003943	1.003520
	0.5	0.2	−1.441522	−1.441520	1.040756	1.040756
		0.3	−1.343664	−1.343664	1.066060	1.066060
		0.5	−1.069109	−1.069109	1.119838	1.119838
		0.7	−0.701535	−0.701539	1.174081	1.174081

Table 1. Values of skin friction coefficient $\mathrm{Re}_x^{1/2}C_\mathrm{f}$ and local Nusselt number $\sqrt{\frac{2L}{x}}\mathrm{Re}_x^{-1/2}\mathrm{Nu}_x$ for different values of K and Γ when $\lambda = 0.1$ and $\mathrm{Pr} = 1$.

ingly steeper when Pr is increased. Therefore the local Nusselt number, being proportional to the initial slope, increases with an increase in Pr.

The numerical values of the skin friction coefficient and the local Nusselt number have been tabulated in Table 1. The values are computed by both HAM and shooting method. We found that a larger drag force is required to displace the fluid over an exponentially stretching sheet when compared to the linearly stretching sheet. The magnitude of the skin friction coefficient significantly increases with an increase in K. However there is a decrease in the coefficient of skin friction when Γ is increased. From the industrial point of view this is a useful result since the power generation involved in displacing the fluid over the sheet can be reduced by assuming larger values of Γ. In accordance with the observations noted in [9] for a linearly stretching sheet, the magnitude of the skin friction coefficient significantly decreases with an increase in the velocity ratio λ. We already noticed that the thermal boundary layer thickness decreases when K is increased. This results in a larger rate of heat transfer at the stretching sheet. Further the magnitude of the local Nusselt number slightly decreases with an increase in Γ.

6. Conclusions

Boundary layer flow and heat transfer of a Powell–Eyring fluid in the region of stagnation point towards an exponentially stretching sheet are investigated. The developed mathematical problems have been solved for the series solutions by the well-known homotopy analysis method (HAM). A very good averaged residual is found at only 15th-order of approximations. The HAM solutions are also found in excellent agreement with the obtained numerical solution. We noticed that velocity and boundary layer thickness increase with an increase in the rheological fluid parameter K. This increase accompanies with larger wall shear stress. On the other hand velocity and skin friction coefficient are

decreasing functions of dimensionless fluid parameter Γ. The results indicate that the drag force in displacing the fluid over an exponentially stretching sheet is larger than that over a linearly stretching surface. Moreover temperature and thermal boundary layer thickness decrease with an increase in K and Pr. This reduction gives rise to the rate of heat transfer at the sheet. The series solutions for the case of Newtonian fluid which are not yet computed can be obtained by choosing $K = 0$.

Acknowledgement

The research of Dr. Alsaedi was partially supported by the Deanship of Scientific Research (DSR), King Abdulaziz University, Jeddah, Saudi Arabia.

[1] N. T. M. Eldabe, A. A. Hassan, and M. A. A. Mohamed, Z. Naturforsch. **58a**, 204 (2003).
[2] J. Zueco and O. A. Beg, Int. J. Appl. Math. Mech. **5**, 1 (2009).
[3] S. Islam, A. Shah, C. Y. Zhou, and I. Ali, Z. Angew. Math. Phys. **60**, 1178 (2009).
[4] M. Patel and M. G. Timol, Appl. Numer. Math. **59**, 2584 (2009).
[5] T. Hayat, Z. Iqbal, M. Qasim, and S. Obaidat, Int. J. Heat Mass Trans. **55**, 1817 (2012).
[6] B. C. Sakiadis, AIChE J. **7**, 26 (1961).
[7] L. J. Crane, Z. Angew. Math. Phys. **7**, 21 (1961).
[8] K. R. Rajagopal, T. Y. Na, and A. S. Gupta, Rheol. Acta **23**, 213 (1984).
[9] T. R. Mahapatra and A. S. Gupta, Int. J. Nonlin. Mech. **39**, 811 (2004).
[10] R. Cortell, Chem. Eng. Process. **46**, 721 (2007).
[11] N. Bachok, A. Ishak, and I. Pop, Phys. Lett. A **374**, 4075 (2010).
[12] S. Abbasbandy and H. R. Ghehsareh, Int. J. Numer. Meth. Fluids **70**, 1324 (2012).
[13] T. Fang, J. Zhang, and Y. Zhong, Appl. Math. Comput. **218**, 7241 (2012).
[14] T. Hayat, M. Mustafa, and A. A. Hendi, Appl. Math. Mech. – Engl. Ed. **32**, 167 (2011).
[15] M. Mustafa, T. Hayat, and A. A. Hendi, ASME-J. Appl. Mech. **79**, 021504 (2012).
[16] M. Mustafa, T. Hayat, and S. Obaidat, Z. Naturforsch. **67a**, 70 (2012).
[17] K. Bhattacharyya and G. C. Layek, Int. J. Heat Mass Trans. **54**, 302 (2011).
[18] E. Magyari and B. Keller, J. Phys. D. Appl. Phys. **32**, 577 (1999).
[19] E. M. A. Elbashbeshy, Arch. Mech. **53**, 643 (2001).
[20] S. K. Khan and Sanjayanand, Int. J. Heat Mass Trans. **48**, 1534 (2005).
[21] M. Sajid and T. Hayat, Int. Commun. Heat Mass Trans. **35**, 347 (2008).
[22] S. Nadeem, T. Hayat, M. Y. Malik, and S. A. Rajput, Z. Naturforsch. **65a**, 495 (2010).
[23] S. J. Liao, Commun. Nonlin. Sci. Numer. Simul. **14**, 983 (2009).
[24] S. J. Liao, Commun. Nonlin. Sci. Numer. Simul. **15**, 1421 (2010).
[25] S. J. Liao, Commun. Nonlin. Sci. Numer. Simul. **15**, 2003 (2010).
[26] S. Abbasbandy and A. Shirzadi, Commun. Nonlin. Sci. Numer. Simul. **16**, 112 (2011).
[27] S. Abbasbandy, Nonlin. Anal. Real World Appl. **11**, 307 (2010).
[28] A. S. Bataineh, M. S. M. Noorani and I. Hashim, Commun. Nonlin. Sci. Numer. Simul. **14**, 1121 (2009).
[29] T. Hayat, M. Mustafa, and S. Asghar, Nonlin. Anal. Real World Appl. **11**, 3186 (2010).
[30] M. Mustafa, T. Hayat, I. Pop, S. Asghar, and S. Obaidat, Int. J. Heat Mass Trans. **54**, 5584 (2011).
[31] M. Mustafa, T. Hayat, and S. Obaidat, Meccanica **47**, 1581 (2012).
[32] S. Nadeem, A. Hussain, and M. Khan, Commun. Nonlin. Sci. Numer. Simul. **15**, 475 (2010).
[33] R. Mahmood, S. Nadeem, and N. S. Akbar, J. Taiwan Inst. Chem. Eng. **44**, 586 (2013).
[34] M. Y. Malik, A. Hussain, and S. Nadeem, Scient. Irani. **20**, 313 (2013).
[35] T. Hayat and M. Nawaz, J. Taiwan Inst. Chem. Eng. **42**, 41 (2011).
[36] S. J. Liao, Homotopy Analysis Method in Nonlinear Differential Equations, Springer, Berlin, Heidelberg 2012.